Recombination Reactions and Diffusive Properties of Diatomic Molecules in Two Different Microporous Structures: Silicalite and ZK4

Pierfranco Demontis,* Giuseppe B. Suffritti, and Antonio Tilocca

Dipartimento di Chimica, Universita' degli studi di Sassari, Via Vienna 2, I-07100 Sassari, Italy

Received: May 7, 1999

Computer simulations of the dissociation−recombination reaction of diatomic molecules have been carried out in the pore networks of the zeolites silicalite and ZK4. This kind of processes can provide interesting insights into the effect of the confinement on the reaction dynamics. The diffusion of the species involved in the recombination processes has been separately investigated through equilibrium simulations. Considerable differences between silicalite and ZK4, both in the recombination probability and in the relaxation rate of excited molecules, as well as in the diffusive properties, are discussed and interpreted on the basis of the different properties of the two environments.

1. Introduction

The catalytic action of zeolites has been the subject of considerable experimental and theoretical activity.[1−3] The selectivity of the reactants, the selectivity of products, and the very chemical effect of acid−base and/or transition-metal catalysis are peculiar to this class of materials. In a schematic representation of the catalytic event the reactants enter the pores of the zeolite and move constrained by the force field of the pore system. Then they may be sorbed at an active site and eventually converted to products that finally are desorbed and transported away from active sites. Each of these steps is strongly influenced by the composition and constitution of the framework structure and also by the geometric properties of the void space that makes up the porous volume within the crystal. The idea that the continuous interactions of the sorbate molecules with the walls of the adsorbent can influence the reactivity of the sorbed species is validated by the fact that the framework can dissipate the excess energy of a chemical process or furnish thermal energy to reactants or products.[3] Therefore the mechanism of energy exchange between the sorbate molecule and its surrounding framework is one of the major subjects in order to understand chemical reactions in zeolites.[4] In recent years the development of a frequency-tunable and high-power infrared laser source has provided access to picosecond and faster time scale processes.[5] In fact, experimental progress in this area has enabled the real-time measurement of vibrational relaxation of the species adsorbed on oxide surfaces with an increasing interest in the surface of zeolites.[6] In this field, computer simulation experiments can be complementary to supplement the available information about the energy transfer pathway. In the present work we apply classical molecular dynamics (MD) calculations to the study of the recombination reaction of photodissociated halogen radical species in two different zeolite topologies: silicalite and ZK4. They are the all-silica analogues of synthetic zeolites ZSM-5 and A respectively, which are of considerable interest for their widespread applications.[1] Their topologies are different enough to allow the exploration of many characteristic zeolite properties; the simulations of their all-silica forms turn out to be much easier, due to the absence of aluminum and thus of charge-compensating cations and/or protons.

We also separately investigate the diffusive properties, in the same environments, of the atomic and molecular species involved in the reactions. In this report we will not attempt a direct comparison with the available experimental data on photodissociation−recombination reactions of halogens in condensed phases or in compressed rare gas cages.[7−14] This class of reactions is used here mainly as a probe to explore the diverse dynamical response of the two zeolites, without considering the exact reaction dynamics, whose simulation would not be feasible with the simple model adopted to make the calculations viable. Indeed, we do not consider the participation of excited electronic states in the dissociation−recombination process; the curve-crossing dynamics should be included in the simulations in order to achieve a more detailed description of the exact reactive dynamics,[15,16] but we preferred to model the recombination as occurring on a single electronic surface because this simplification allows longer simulation times, which are required to reach the main purpose of our study.

The photochemistry of compounds adsorbed in zeolites, exploiting many of their specific properties, results in a particularly suitable starting point to obtain comparative information on the catalytic activity of different zeolitic hosts. Indeed, in solution, the properties of the solvent, such as polarity and viscosity, determine the photochemical behavior of the system to a great extent and likewise any intrazeolite photochemistry is influenced by the zeolite environment.[17−24] The confinement within the cavities of zeolites determines the fate of the reactants and radicals formed upon irradiation by restricting their relative mobilities. For example, while in solution the intermediate radicals readily diffuse apart to form coupling products in statistical ratios, in many cases the zeolite could severely inhibit the radicals' movement (hindering their out-of-cage diffusion, which would lead to random radical coupling); therefore only the geminate cage recombination products are often found.[25,26] Moreover, the mobility restrictions and size-selectivity of zeolites can considerably differ from each other and lead to different product distribution after the photochemical excitation.[27] The protective power of the zeolite cavities may stabilize transient species that would have much shorter lifetimes when

* Corresponding author.

10.1021/jp991449l CCC: $18.00 © 1999 American Chemical Society
Published on Web 09/08/1999

generated in solution,[28] thus allowing new reaction pathways involving these transients. The zeolite active sites can in some cases directly and actively cooperate in the success of a photochemical reaction.[29] All these effects are rather complex; however, they are undoubtedly involved in many general aspects of the zeolite catalytic activity. As detailed knowledge of the mechanism of most chemical reactions in zeolites is still lacking,[30−32] an investigation of dissociation−recombination processes at the molecular level could provide some general insights into basic features of the zeolite activity. The method and potentials adopted here to model the recombination of photodissociated, spherical species, are clearly too simplified to allow exact, quantitative data to be extracted. At the same time, they are general enough to allow a straightforward and consistent extension to different sorbate/adsorbent pairs. In our opinion, as long as the *comparison* between the properties of zeolite hosts is the main goal, the peculiar features of photodissociation−recombination processes, together with the proposed method to model them, could represent a very suitable approach to follow.

It should be noted that the dissociation−recombination of iodine, after becoming a prototype for investigating such kind of processes in various environments,[33,34] has recently received new interest for the study of femtochemistry in nanocavities,[35,36] consolidating our interest to exploit these processes to address the more general effects of a confined geometry on the reaction dynamics.

2. Computational Model and Details

Recently[37] we applied MD simulations to the study of the recombination reaction between two photodissociated atoms occurring in a silicalite-type zeolite and in a liquid solvent. The model and the method adopted there are the same used in the present work. A stable diatomic molecule is induced to dissociate by rescaling the velocities of both atoms in such a way to increase the internal energy of the molecule above the dissociation limit. The fate of the photodissociated fragments is then followed by integrating the Newtonian equation of motion for further 60 ps; 200 such trajectories, each one starting from a different equilibrated configuration, are integrated and analyzed for each case. In the previous work, the two radicals always interacted via a Morse potential, with parameters corresponding to the electronic ground state of the iodine molecule; accordingly, the mass of each atom was 126.9 amu, and the parameters for the Lennard−Jones interaction between the radicals and the zeolite oxygen atoms were the same as Xe−O. We remarked elsewhere that this model is far too simplified to describe the complex features of the specific, real iodine dissociation−recombination reaction, but it may be suitable if the only purpose is to gain information about the zeolite action and its effectiveness in promoting atom recombination. In other words, the results obtained (recombination rates and yields) should be observed from a more general, qualitative point of view, i.e., only to explain and better understand some features of the zeolite catalytic action. From this perspective, the comparison between the recombination process of different diatomic species in different zeolite structures may give further insight into the basic properties of zeolite structures and their influence on the mechanism of radicalic reactions.

We chose to examine here two completely different all-silica zeolites: silicalite[38] and ZK4[33]. The first one has an highly anisotropic structure (Figure 1a) made of straight channels intersecting orthogonally with sinusoidal channels, both with a diameter of about 5.5 Å (the intersections diameter is about

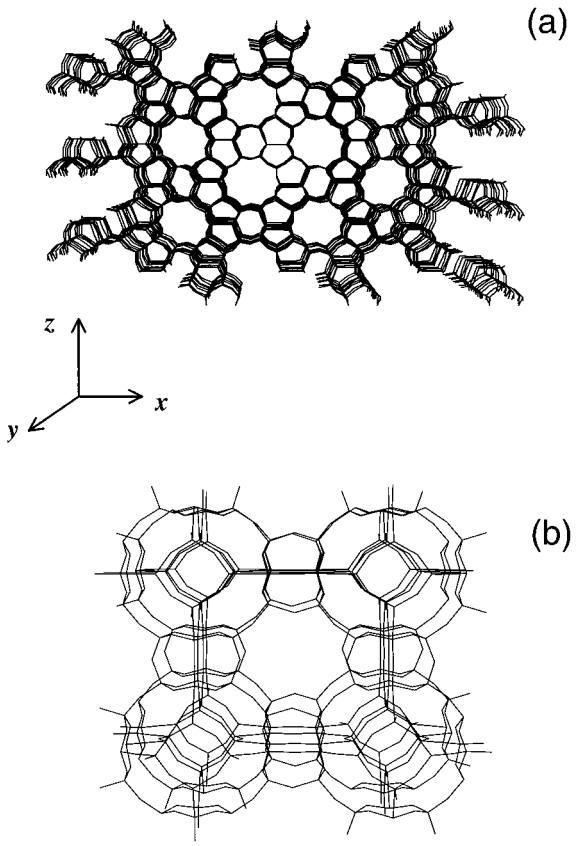

Figure 1. (a) Structure of silicalite, view along the straight channels. (b) Structure of ZK4, showing the central α-cage.

TABLE 1: Potential Parameters Used

Lennard−Jones[a] Interactions

interaction	σ (Å)	ϵ (kJ mol^{-1})
Cl−O	3.029	1.028
Br−O	3.14	1.335
I−O	3.2745	1.737

Morse Potential[b] Paramaters

	r_{eq} (Å)	β (Å^{-1})	D (kJ mol^{-1})
Cl_2	1.988	2.037	242.19
Br_2	2.28	1.964	192.044
I_2	2.666	1.867	148.703

Harmonic Potential[c] Parameters (zeolite atoms)

$k_{Si-O} = 2092$ kJ mol^{-1} Å^{-2};
$r_{eq,Si-O} = 1.605$ Å
$k_{O-O} = 430.952$ kJ mol^{-1} Å^{-2};
$r_{eq,O-O} = 2.618$ Å

[a] $V(r) = 4\epsilon\,[(\sigma/r)^{12} - (\sigma/r)^6]$. [b] $V(r) = D\{[1 - \exp(-\beta\,(r - r_{eq}))]^2 - 1\}$. [c] $V(r) = 1/2\,k\,(r - r_{eq})^2$.

9 Å); on the other hand, the ZK4 microporous structure (Figure 1b) is made of large spherical cages (diameter ∼ 11.4 Å) connected by narrow windows of about 4.2 Å, and arranged in a simple cubic lattice; each ZK4 unit cell contains 8 large cages. The recombination of three diatomic molecules has been investigated; the Morse and LJ parameters modeling their intra- and intermolecular interactions (Table 1) roughly represent the halogen molecules, chlorine, bromine, and iodine, and in the following they are referred to as Cl_2, Br_2, and I_2. Note that the interaction parameters for Cl−O, Br−O, and I−O are the same

as Ar−O, Kr−O, and Xe−O, respectively.[40,41] No direct interactions between the halogen and Si atoms are considered, as usual in MD simulations of zeolites, because it is assumed that the silicon atoms are effectively screened by the larger and more polarizable oxygen atoms covering the surface of cavities.

The Morse potential parameters have been extracted from ref 42 with some slight adjustments according to more recent data.[43,44] The motion of the silicate framework was modeled by an effective potential,[45] with harmonic springs connecting nearest-neighbors atoms, including both silicon−oxygen and oxygen−oxygen pairs. This simple harmonic force field has been shown to reliably represent the energy-exchange effects between the framework and the guest species.[46,47]

Silicalite crystal structure was represented[38] in the *Pnma* space group (orthorombic), with unit cell lattice parameters $a = 20.022$ Å, $b = 19.899$ Å, $c = 13.383$ Å, while ZK4 was represented in the $Fm\bar{3}c$ space group ($a = 24.555$ Å), the same as for the NaA zeolite.[39] The simulation box consisted of $2 \times 2 \times 2$ unit cells for both silicates, including 4608 framework atoms (1536 Si and 3072 O) for ZK4, and 2304 for silicalite. The cutoff distance for the oxygen−halogen atom interactions was 9 Å, while there is no cutoff for the interactions between the two radicals.

The adsorbent systems were chosen to be considerably large, so as to avoid spurious recombinations due to the application of the periodic boundary conditions (PBC): if the distance between the two atoms exceeded $L/2$ (L being the side of the simulation box), the scaling implicit in the PBC would bring them close again, thus altering the recombination dynamics. This is the reason for adopting large enough values of L, together with an "outer cutoff" distance beyond which the trajectories are ended (vide infra). Moreover, the inclusion of a larger portion of the silicate framework in the simulation undoubtedly leads to a more realistic description of the overall action exerted by the host on the guest species.

The equations of motion were integrated by using a modified version of the Verlet algorithm,[48] with a time step of 1.0 fs. The simulations were performed in the microcanonical ensemble at the run temperature of 300 K.

An initial relaxed configuration was created by introducing a stable diatomic molecule in the interior of the zeolite framework and then equilibrating the system (by rescaling all atom velocities at every time step) to the desired temperature for 200 ps. The final thermalized configuration was the starting point for the first trajectory; the equilibrated molecule was allowed to diffuse freely for a 10 ps interval, at the end of which the system configuration was stored; then, dissociation was induced and the dynamical evolution of the system was followed. The next trajectory was started from the previously stored configuration, and the same procedure (free molecular diffusion for 10 ps, storage, dissociation, and reactive dynamics study) was repeated. In this way, it has been possible to examine many distinct reactive trajectories, because in each one the dissociation was carried out in different regions of the zeolites. Indeed, we verified that in the "free diffusion" regime preceding all dissociations the initial diatomic molecule considerably moved inside the pore network of the zeolite, thus most part of the zeolite-molecule initial configurations, and practically all the available void space have been explored.

The energy needed to induce the dissociation is obviously different for the three molecules, as the corresponding Morse well depths are different (see Figure 2). To achieve a comparable description of the dissociative event in the three cases, the excess kinetic energy (given by $E_{diss} - D_e$, where E_{diss} is the kinetic energy furnished to break the bond, and D_e is the Morse dissociation energy) was kept equal to the value previously adopted for the iodine,[37] i.e., 77 kJ mol^{-1}. In this way the two atoms, after having escaped from their Morse well, should have similar kinetic energies in all cases, and their subsequent dynamics should be driven only by the topology and the energetics of the environment.

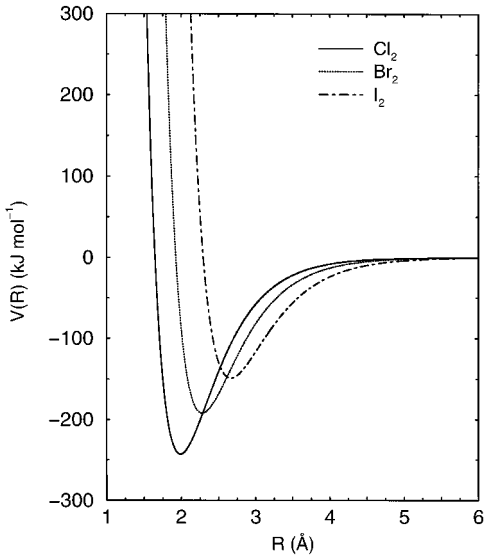

Figure 2. Morse potential curves for the three halogens studied.

2.1. Classification of Trajectories. Useful data on the effects of a particular zeolite topology can be obtained by distinguishing the specific kinds of recombinative and dissociative events observed in each environment. This classification can be made on the basis of cutoff distances fixed on empirical basis. For the iodine case, an inner cutoff distance R_{ic} of 4.3 Å was determined by direct inspection of the trajectories;[37] when the two dissociated radicals came closer than this value, recombination was considered to have occurred, provided that they did not redissociate later. The possibility of a later redissociation was accounted for by fixing a secondary cutoff R_{sc} at 4.8 Å, which is the "external bound" for the reaction; if, after colliding, the two atoms were not able to dissipate the excess vibrational energy and their distance again exceeded 4.8 Å, a redissociation event was accounted for. When we turn to another diatomic species, the Morse potential determining the recombinative dynamics is much different (Figure 2), so that the cutoff values need to be consequently adjusted. We adopted the following criterion: since $V_{Morse}(R_{ic}) = -5.5\ k_B T$, and $V_{Morse}(R_{sc}) = -2.2\ k_B T$ at $T = 300$ K for iodine, we chose the cut-off values for chlorine and bromine in such a way to respect the same relations, thus obtaining $R_{ic} = 3.73$ Å, $R_{sc} = 4.18$ Å for chlorine, and $R_{ic} = 3.97$ Å, $R_{sc} = 4.44$ Å for bromine. It should be remarked that these values are not crucial for the interpretation of results, as the ultimate fate of a trajectory (reactive or nonreactive) is absolutely independent of them, but they are very useful in the distinction of different recombination routes. For example, we are able to distinguish a *simple* reaction from a *complex* one on the basis of the observed number of crossings of the cutoffs. A simple recombination takes place at the first encounter between atoms; after crossing R_{ic}, their fall into the Morse well is quick and irreversible, and only one crossing of R_{ic} is observed in the trajectory. Instead, in a complex reaction, after the first crossing, the recombined atoms do not thermalize and shortly escape again from the Morse well; at this point they can recombine again, or definitively separate. In both cases several crossings of the critical distances R_{ic} and R_{sc} are observed, but in the first case

TABLE 2: Event Percentages (calculated over 200 trajectories)

	silicalite				ZK4			
reactive	TOT	S	RDR	C	TOT	S	RDR	C
Cl_2	40.5	27	9	4.5	46.5	22.5	23.5	0.5
Br_2	33	21	10	2	51	24	27	0
I_2	35	22	8.5	4.5	64	26	37.5	0.5
nonreactive	TOT	RD	OC	N	TOT	RD	OC	N
Cl_2	59.5	7.5	52	0	53.5	18	35.5	0
Br_2	67	3	64	0	49	16	33	0
I_2	65	5	59.5	0.5	36	14	22	0

a final, complex reaction is recorded, while the latter case is classified as *dissociative* recombination. Another possible (and, actually, rather common) event is the immediate and definitive separation of the two radicals following the initial dissociation; when the distance between the two dissociated fragments reached an *outer cutoff* of 13 Å, a later encounter was rather unlikely on the examined time scale (60 ps) and the trajectory was terminated. To sum up, the possible events accounted for have been divided in two major groups: reactive (i.e., ending in the stabilization of the recombined molecule), and nonreactive (i.e., ending with the two radicals separated). Within these two groups, we adopted the following abbreviations.

Reactive Events. S stands for simple reactions (showing a single crossing of the inner cutoff). RDR stands for complex reactions (the final recombination is preceded by several crossings of R_{ic} and R_{sc}). C stands for caged reactions, i.e., reactions in which the two atoms never separate by more than R_{ic}, so that the molecule actually failed to dissociate, probably because at the dissociation time it was placed in an unfavorable position, or in a very confining site. Indeed, such events are present almost exclusively in the more confining silicalite (Table 2).

Nonreactive Events. RD stands for dissociative recombinations (the final dissociation is preceded by several crossings of R_{ic} and R_{sc}). OC stands for trajectories in which the two radicals reach the outer cutoff distance *directly* after the initial dissociation. N stands for trajectories in which none of the previous events has been recorded: i.e., in the 60 ps following the initial dissociation the two radicals do not recombine nor reach the outer cutoff (actually, this category is basically equivalent to the previous one, but very few trajectories fall into it; this fact shows the adequacy and completeness of the classification criteria adopted).

The percentages of the above-mentioned events observed in the 200 trajectories carried out for each system are reported in Table 2.

2.2. Recombination Times and Collisions. The time interval t_{FE} between the initial dissociation and the first encounter of the two fragments has been averaged over all trajectories, obviously excluding those labeled "*C*", for which an encounter is not clearly defined, and the "OC" and "*N*" ones, which do not lead to any encounter. Moreover, the time t_{REA} between the initial dissociation and the last, final crossing of the inner cutoff has been averaged over all reactive events; obviously its value is larger than t_{FE}, due to the contribution of complex reactions, in which multiple collisions are needed before the final recombination; Table 3 reports the calculated times.

The collisions of the zeolite oxygen atoms with the dissociated radicals, as well as with the atoms of the diatomic molecule, have been recorded in the first picosecond following (a) the initial dissociation, and (b) the eventual recombination (if any). A collision was accounted for whenever the distance between

TABLE 3: First Encounter and Recombination Times

	silicalite	ZK4
	t_{FE} (ps)	
Cl_2	1.1 ± 0.2	0.90 ± 0.06
Br_2	1.8 ± 0.3	1.20 ± 0.07
I_2	1.6 ± 0.2	1.32 ± 0.07
	t_{REA} (ps)	
Cl_2	1.9 ± 0.4	2.4 ± 0.2
Br_2	4.3 ± 0.8	3.4 ± 0.3
I_2	4.0 ± 0.7	4.4 ± 0.4

TABLE 4: Guest−Host Collisions

	silicalite		ZK4	
	after dissociation	after recombination	after dissociation	after recombination
	Frequency (ps^{-1})			
Cl_2	19.7 ± 0.8	15.0 ± 1.1	13.9 ± 0.5	6.3 ± 0.7
Br_2	16.8 ± 1.4	11 ± 1	12.7 ± 0.5	9.2 ± 0.8
I_2	13.1 ± 0.6	9.1 ± 0.8	14.0 ± 0.5	7.7 ± 0.7
	Duration (fs)			
Cl_2	81.7 ± 1.7	66 ± 3	90.0 ± 1.8	65 ± 4
Br_2	103.2 ± 2.4	71 ± 6	113 ± 3	80 ± 6
I_2	96 ± 3	67 ± 4	121 ± 3	81 ± 6
	ΔE per Collision (kJ mol^{-1})			
Cl_2	26.2 ± 1.3	7.5 ± 1.2	25 ± 2	15.2 ± 2.3
Br_2	26.3 ± 2	5.6 ± 1.5	21.6 ± 1.8	10.6 ± 1.8
I_2	20.0 ± 1.2	5 ± 1	14.9 ± 0.9	7.6 ± 1.6
	Dissipation Rate (kJ mol^{-1} ps^{-1})			
Cl_2	516 ± 33	112 ± 20	346 ± 30	96 ± 18
Br_2	442 ± 49	62 ± 17	274 ± 25	97 ± 19
I_2	262 ± 20	45 ± 10	209 ± 15	58 ± 12

two atoms fell below the corresponding LJ parameter σ, i.e., when the interaction energy became positive. The frequency, duration (i.e., the time interval when the distance remained less than σ) and total energy loss were averaged over all guest−host collisions, and are reported in Table 4. Note that the "after dissociation" ΔE refers to the average kinetic energy lost by the two radicals in the collisions after the initial dissociation, while in the other case ΔE represents the total internal energy lost by the formed molecule in the collisions after the recombination. The reported dissipation rate is simply the product of ΔE times the collision frequency.

A better comparison between the features of the energy exchanges in the different guest−host systems could be made by directly observing the dissipation of the excess energy, both for the radicals and for the newly formed molecule. In the first case, the total kinetic energy of the two atoms following the dissociative shock has been averaged over the trajectories in which the two atoms remain separated for at least 2 ps before eventually recombining or reaching the outer cutoff. Figure 3a−c shows the trend observed for chlorine, bromine, and iodine atoms, respectively. In the molecular case, the vibrational energy, defined in eq 1, has been accounted for:

$$E_{vib} = \frac{1}{4}m\left[\left(v_1 \cdot \frac{\boldsymbol{R}}{R}\right) - \left(v_2 \cdot \frac{\boldsymbol{R}}{R}\right)\right]^2 + V(R) \qquad (1)$$

where m is the atomic mass, v_i is the velocity vector of the ith atom, $\boldsymbol{R}$ is the bond vector, and $V(R)$ is the Morse potential energy of the molecule. The curves shown in Figure 4a−c have been obtained by averaging E_{vib} over all the simple reactions, for the 50 ps following the encounter between the two radicals. The other (complex) reactions could not have been included in the average because they would have complicated the interpretations of results, due to the multifarious encounter−separation

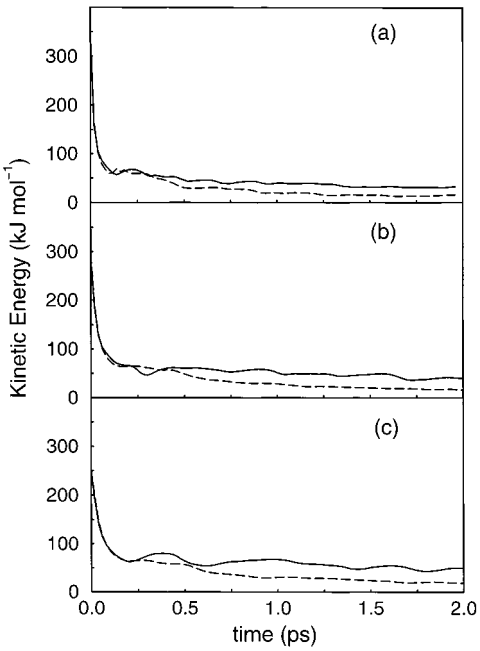

Figure 3. Total kinetic energy of the radicals in the first 2 ps following the initial dissociation of the diatomic molecule: (a) Cl_2; (b) Br_2; (c) I_2. Dashed lines: silicalite; continuous lines: ZK4.

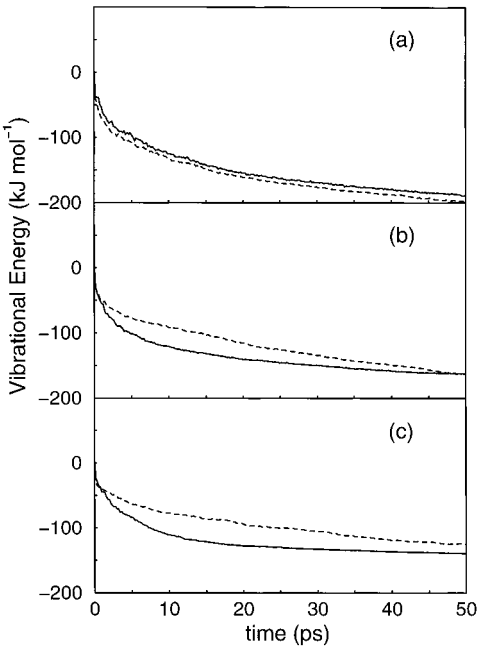

Figure 4. Total vibrational energy of the diatomic molecule in the 50 ps following recombination for (a) Cl_2; (b) Br_2; (c) I_2. Dashed lines: silicalite; continuous lines: ZK4.

cycles (at varying times) between the first encounter and the final recombination.

To investigate possible coupling effects between the vibrational modes of the framework and the oscillation of the diatomics, the IR spectra of silicalite and ZK4, as reproduced by our model, have been derived from the Fourier transform of the total velocity autocorrelation function (VACF), and they are shown in Figure 5. The (equilibrium) oscillation frequencies of Cl_2, Br_2, and I_2 are 565 cm, 323 cm, and 214 cm^{-1} respectively, but it should be remarked that, as the recombination gives rise to a vibrationally excited molecule near the dissociation limit, its frequency may be considerably lower than the equilibrium value.[49] The thermalization of the excited oscillator

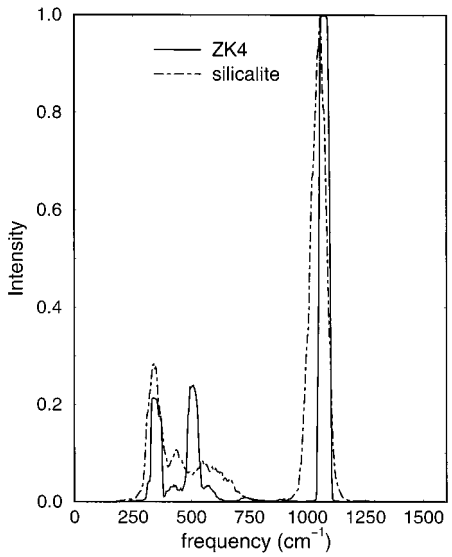

Figure 5. Vibrational spectra of silicalite (dash−dotted line) and ZK4 (continuous line).

will bring it down to the lower portion of the Morse curve, where the equilibrium frequency will be finally matched. This point might have an important influence on the resonance effects with the framework, which are known to be crucial in the stabilization of the excited molecule,[46] and therefore in the overall recombination process.

3. Results and Discussion

3.1. Recombination Probability. Table 2 shows a considerable influence of the host topology on the fate of the dissociated atoms, and on the probability of recombination; in the iodine case, ZK4 leads to a 29% increase of reactive trajectories compared to silicalite, while the increase is 18% for bromine and only 6% for chlorine. This trend is mostly brought about by steric effects; the narrow windows of ZK4 hinder the passage of a large iodine atom, thus often preventing the definitive separation of radicals, which are kept in the same cage. The structure of silicalite, on the other hand, does not show comparable narrow passages, and the definitive dissociation of radicals is easier. The sort of "caging" in ZK4 is obviously less effective for the smaller Br and Cl atoms, whose escape through the windows is consequently easier. The considerable difference in the OC event percentages between silicalite and ZK4 (such events being less probable in ZK4) also reflects these points: there is a 38% difference for iodine, 31% for bromine, and 17% for chlorine. It is interesting to note that Br and Cl atoms show a similar ability to escape from the ZK4 α-cage (i.e., similar percentages of OC events in ZK4), while in silicalite the chlorine unexpectedly gives rise to the least percentage of OC's (also lower than iodine), despite its low weight and dimensions, which should favor the separation of the radicals. Obviously effects other than simple steric considerations come into play in this case; after the dissociation, an ineffective dissipation of the excess kinetic energy of radicals may assist their definitive separation (up to the outer cutoff distance), especially in the less-confining structure of silicalite. Therefore the behavior observed in silicalite could be due to the better dissipation of the excess energy of chlorine atoms (whose mass is closer to that of the framework oxygens, compared to the Br and I masses), which prevents a larger number of outer cutoff events from being recorded, and, at the same time leads to a higher number of reactive trajectories. In other words, in ZK4 the steric

effects have a greater influence on the dynamics, through the cage-like action discussed before, and lead to the order $I_2 > Br_2 > Cl_2$ for the recombination yield. In silicalite, steric effects are less important, and chlorine shows the highest recombination percentage, because of the less probable separation of Cl atoms, which quickly dissipate their excess kinetic energy; the enhanced rotational freedom of Cl_2 in the silicalite channels, compared to Br_2 and I_2, may also be involved in this point (see paragraph 4). We also note that, with the present model, both the dissociation energy and the equilibrium bond length of the Morse oscillator may have some influence on the reaction dynamics. Indeed, they determine the range of the attractive force between the two atoms, which increases going from chlorine to iodine. Therefore, in principle, the iodine recombination could be favored by the longer range of the attractive force between the two radicals. However, our results show that the action of the environment plays the dominant role in the recombination dynamics by means of both steric and energetic effects.

A more exact interpretation can be made looking at the collision parameters of Table 4. The energy loss *per collision* immediately after the dissociation is about 26 kJ mol^{-1} in silicalite, both for Cl and Br, but the higher frequency of collisions for chlorine leads to a higher dissipation rate. Note that also in ZK4 chlorine shows the better dissipation mechanism after the dissociation, but in this case the steric effects are dominant.

Table 4 and Figure 3 show that the energy dissipation of the excited radicals is always more effective in silicalite than in ZK4; after the dissociation a greater amount of energy is lost in silicalite in all cases. An immediate consequence of this fact is that, whenever the two radicals collide, the initial energy of the newly formed diatomic should be lower in silicalite; we directly verified this hypothesis—the initial vibrational energy was averaged over all encounters, and the mean values obtained for silicalite in all the three cases were 8−10 kJ mol^{-1} lower than for the encounters in ZK4. As the two radicals collide with a lower initial energy the subsequent stabilization of the molecule will be easier and a higher probability for the "simple" reactions in silicalite should result, regardless of the effectiveness of the following vibrational relaxation. Indeed, the ratio of simple reactions to total encounter numbers (defined as S/[S + RDR + RD]) is about 62% for silicalite and 33% for ZK4 (surprisingly, these ratios are practically unchanged for all the three species considered): therefore, notwithstanding the different effectiveness of the two silicates in the stabilization of the formed molecules (which is pointed out below), the effect of the initial energy of the diatomic molecule, which is higher in ZK4, is of greater importance in the recombination dynamics. In other words, as long as the encounters occur between two highly excited atoms, the outcome of each encounter is determined mostly by the initial energy (depending on the dissipation rate *following dissociation*) and to a smaller extent by the relaxation route following the collision. Another point in favor of this hypothesis is that the fraction of ineffective encounters ending in a dissociation, (RD/[S + RDR + RD]), is considerably higher in ZK4, for all cases considered. This happens mainly because in ZK4 the nascent molecules are characterized by a considerably higher initial vibrational energy, which often induces their subsequent redissociation.

3.2. Recombination Rates. For each halogen, the different environment does not seem to affect considerably the rate of first encounter and of recombination: no marked differences exist between the t_{FE}'s in silicalite and in ZK4 (Table 3), as well as between the t_{REA}'s, for each of the three sorbates (only for bromine both the first encounter and the final reaction seem to occur slightly faster in ZK4). This could confirm that, for this class of reactions, the primary recombination *rate* is largely independent of the molecular details of the environment, while on the other hand the recombination *probability* is, to a greater extent, solvent dependent, as pointed out by Schwartz et al.[50] and in our previous paper.[37] The times of final recombination t_{REA} are about three times larger than the times of first encounter t_{FE}, due to the contribution of the complex recombinations, which require more time than the direct, simple ones, for which t_{REA} and t_{FE} clearly coincide. However, some differences arise between the three halogens; the first collision between chlorine atoms is only slightly quicker than for the other two halogens, whereas the final recombination of the Cl_2 molecule is faster than that of Br_2 and I_2, especially in silicalite. This is in line with the preceding discussion; when the first collision occurs, the two chlorine radicals have already transferred to the zeolite a considerable fraction of their excess initial energy, so that the stabilization of the molecule leading to the final recombination is faster.

3.3. Vibrational Relaxation. So far, we have not taken into account the dynamics following the bond formation. A fast vibrational relaxation of the excited molecule should prevent its later redissociation by quickly trapping the molecule in the lower portion of the Morse potential well. The values of Table 4 also tackle this topic; the *single* collisions after recombination are considerably more effective in ZK4, as shown in the larger ΔE (per collision) values. A better vibrational coupling between molecule and framework in the ZK4 case, compared to silicalite, may be due to the sharp band around 500 cm^{-1} in the IR spectrum of ZK4, which should enhance the guest−host energy transfer, especially in the case of chlorine, whose vibrational frequency falls in that region. However, in the overall relaxation phenomenon other system-dependent collisional properties have to be considered; in particular, the collision frequency, which is mainly determined by the topology of the environment, may be taken into account by referring to the dissipation rate, i.e., the energy loss per collision (ΔE) times the collision frequency. For the radical-oxygen collisions after dissociation, the rate of dissipation follows the order Cl > Br > I in both zeolites, strictly corresponding to the better match between the colliding masses. Note that the rate decrease from Cl to Br is comparable in both zeolites, while there is a three times greater decrease in silicalite when we compare the dissipation rates of Br and I. This is an interesting point, as the difference between the Cl−Br masses is very similar to that between Br and I. The rate decrease difference arises from the considerably lower dissipation rate of iodine in silicalite, compared to bromine, which in turn stems from the decrease of *both* the efficiency and frequency of collisions, while in ZK4 only the ΔE per collision significantly decreases. The different structure is most likely involved in the different trends of the collision frequency following dissociation; however, by referring to the dissipation rate alone the interpretation of the collision features is simplified, i.e., one does not need to separately consider their efficiency and frequency, and the main result emerging for the radical−zeolite collisions is the predominant importance of the atomic masses in determining the energy exchange rate.

For the collisions of diatomic molecules, additional resonance and steric effects could take part in the energy exchanges together with the above effects due to the similarity of colliding masses. While in silicalite the order is again $Cl_2 > Br_2 > I_2$, in ZK4 we have $Cl_2 \sim Br_2 > I_2$, due mainly to the low collisional

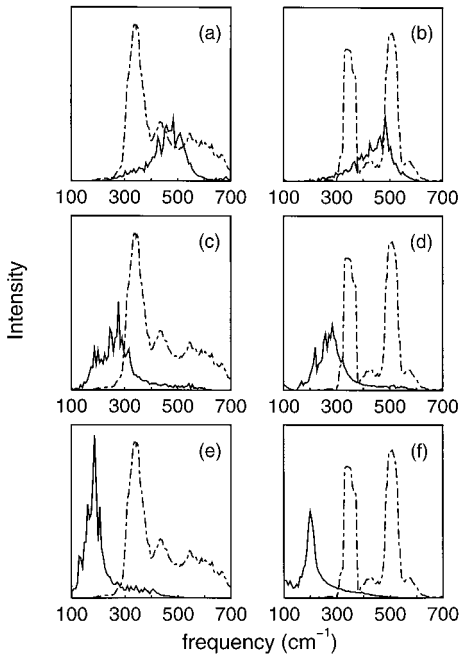

Figure 6. Vibrational spectra of excited diatomic molecules in silicalite and ZK4 (continuous lines). The vibrational spectrum of the host silicate (dash−dotted line) is superimposed to each figure for comparison. (a) Cl_2−silicalite; (b) Cl_2−ZK4; (c) Br_2−silicalite; (d) Br_2−ZK4; (e) I_2−silicalite; (f) I_2−ZK4.

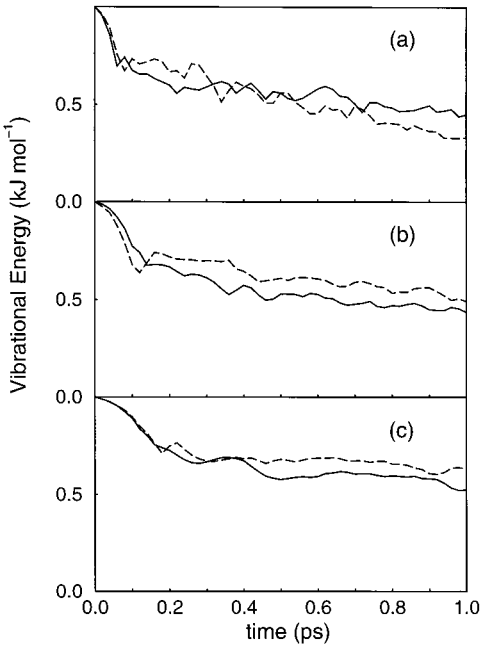

Figure 7. Normalized total vibrational energy curves in the first picosecond following recombination for (a) Cl_2; (b) Br_2; (c) I_2. Dashed lines: silicalite; continuous lines: ZK4.

frequency observed for the relatively small chlorine molecule in such rather wide environment. Turning to the comparison between the silicates, Figure 4 shows that, for chlorine, the vibrational relaxation in the two environments occurs in a similar way: the two vibrational energy loss curves are almost superimposed. For bromine and iodine the vibrational energy of the excited molecule decays faster in ZK4. Further insight into the effect of the guest−host vibrational coupling is given by the velocity spectra of the excited molecules reported in Figure 6. They have been obtained by Fourier transforming the velocity autocorrelation functions of the single atoms of the recombined molecule in the 50 ps following the recombinations. Therefore they could give some hints in the interpretation of the vibrational energy curves that extend to the same time scale. Note that the translational bands (frequency < 100 cm^{-1}) are not shown, as they are not directly involved in the vibrational relaxation; the band shown corresponds to the oscillation of the excited molecule which progressively relaxes to equilibrium. Therefore it extends from the initially lower frequencies to the final equilibrium value.

On one hand, the bands corresponding to the vibration of the excited chlorine molecule and to the low-frequency modes of both silicates considerably overlap, and this could explain the comparable relaxation rates for Cl_2 in the two environments (Figure 4a). On the other hand, for iodine and bromine the molecular vibration band is shifted to lower frequencies and only a weak superimposition is present with the vibrational spectra of *both* zeolites, which does not account for the faster relaxation observed in ZK4 (Figure 4b,c). Therefore it seems that, when a considerable overlap between the frequencies of sorbates and the spectrum of silicates is present, then the resonance phenomena between vibrational modes can be very important in determining the dynamical behavior of the system. When the molecule oscillates at frequencies outside the vibrational spectrum of the zeolite other system-dependent effects, which would otherwise be obscured by the dominant influence of resonance phenomena, can play a crucial role, e.g., the collision frequency that is accounted for by the dissipation rates defined above. Note that the dissipation rates reported in Table 4 only sample the first picosecond following recombination, while the energy curves are representative of 50 ps. Therefore the latter better represent the overall relaxation phenomenon, and we referred to them in discussing the resonance effects. However, the calculated dissipation rates of the newly formed molecule can be directly compared with the vibrational energy curves in the first picosecond following recombination, shown in Figure 7. Note that the reported curves have been normalized to allow a better comparison between the two zeolites because the initial energy of the nascent molecule is always higher in ZK4, as pointed out above. On this short time scale, only chlorine seems to relax slightly faster in silicalite, while the initial energy relaxation in ZK4 is seemingly more effective for bromine and iodine. This is in fair agreement with the "after recombination" dissipation rates of Table 4: even considering the size of the error bars bromine and iodine show higher rates in ZK4, while for chlorine there is a little rate increase in silicalite.

4. Diffusive Properties

The equilibrium diffusive properties of all the guest species (both diatomic molecules and single atoms) involved in the recombination process have been examined in the two hosts considered. In this case the studied systems consisted of one molecule (or atom) and 576 framework atoms (192 Si and 384 O), corresponding to two unit cells (superimposed along z) for silicalite, or one unit cell for ZK4 (the adopted cutoff distance between halogen and oxygen atoms was kept at 9 Å, as before). These simulation boxes are clearly smaller than those adopted in the previous recombination simulations, because in the present case the molecule does not dissociate, and the distance between the two atoms cannot in any case approach values near $L/2$, where L is the side of the simulation box. Thus spurious effects connected to the application of the periodic boundary conditions are absent, and smaller systems (allowing longer simulations) should give reliable results.

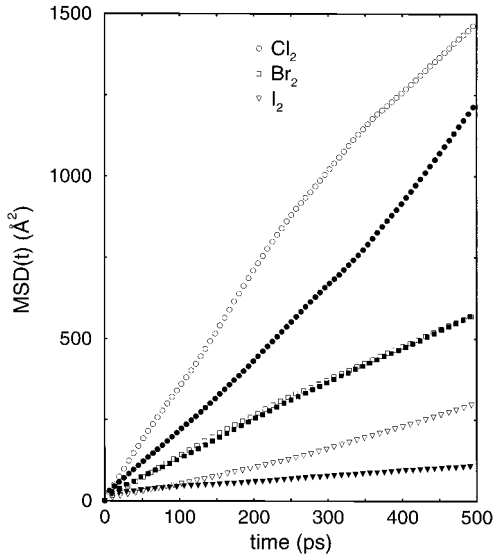

Figure 8. Mean square displacement of diatomic molecules at 300 K; empty symbols: silicalite; filled symbols: ZK4.

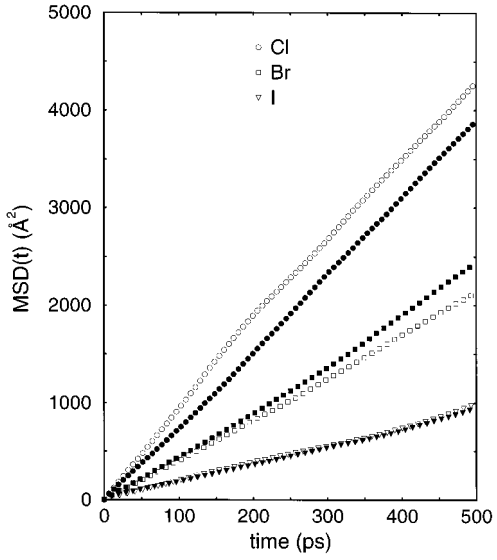

Figure 9. Mean square displacement of atomic species at 300 K; empty symbols: silicalite; filled symbols: ZK4.

In each case the system was equilibrated in the microcanonical ensemble at $T = 300$ K for 90 ps, then a production run of 10 ns was carried out using a time step of 1.0 fs. The fluctuations in the total energy were less than 0.005%. Coordinates and velocities of the diatomic (or of the single atom) were stored every 32 fs for later analysis. The mean square displacement (MSD) of each species was calculated according to eq 2:

$$\Delta r^2(t) = \frac{1}{N_{o t_o=1}} \sum^{N_0} |\boldsymbol{r}_i(t_0 + t) - \boldsymbol{r}_i(t_0)|^2 \qquad (2)$$

where the $\boldsymbol{r}_i$'s are the center of mass coordinates of diatomic molecules, or the single atom coordinates, and the average is over N_0 time origins (only one diffusing species is present). The calculated MSD's are shown in Figure 8 and Figure 9. The diffusion coefficients were calculated according to the well-known Einstein's equation:

$$D = \lim_{t \to \infty} \frac{\Delta r^2(t)}{2dt} \qquad (3)$$

TABLE 5: Diffusion Coefficients (/10^{-9} m^2 s^{-1})

	silicalite	ZK4
Cl_2	5.9 ± 0.7	3.9 ± 0.7
Br_2	1.9 ± 0.5	1.9 ± 0.4
I_2	1.1 ± 0.2	0.28 ± 0.1
Cl	13.9 ± 1.4	13.2 ± 2.6
Br	7.2 ± 2.0	8.2 ± 1.0
I	3.1 ± 0.6	3.0 ± 0.6

TABLE 6: Mean Guest−Host Potential Energies (kJ mol^{-1})

	silicalite	ZK4
Cl_2	−22.7	−14.5
Br_2	−35.1	−21.9
I_2	−55.9	−33.9
Cl	−11.3	−7.4
Br	−17.4	−11.3
I	−27.8	−17.3

where d is the corresponding dimensionality. The MSD curves were linearly fitted in the 50−500 ps range, leading to the diffusion coefficients reported in Table 5. The error bars have been obtained from a block analysis of data[51] by dividing each trajectory in 10 blocks of 1 ns each. The mean potential energies for the guest−host interaction are reported in Table 6. It is interesting to remark that the guest−host interaction energy is always 35−40% larger (more negative) in silicalite for all species, due to the more confining silicalite structure. Indeed, the LJ parameters for the guest−host interactions are the same in the two silicates, so that any difference can only arise from their different topology. As the parameter for the Cl, Br, and I are the same as Ar, Kr, and Xe, the obtained diffusion coefficients and adsorption energies of radicals can be directly compared with experimental and theoretical data.

Heink et al.[52] applied the PFG-NMR technique to study the diffusion of Xe in silicalite, obtaining $D \sim 4 \times 10^{-9}$ m^2 s^{-1} with a loading of 4 atoms/u.c. Frequency-response measurements[53] gave $D \sim 1.1 \times 10^{-9}$ m^2 s^{-1} at concentrations lower than 1 Xe atom per unit cell. These values are in reasonable agreement with our value (3.1×10^{-9} m^2 s^{-1}) for the iodine radical at infinite dilution, considering the not negligible error usually involved in the experimental measurements of the diffusion coefficient. The isosteric heat of adsorption in the limit of zero coverage q_{st}^o of Ar in silicalite has been recently estimated[54] as 15.8 kJ mol^{-1} at room temperature; recalling that $q_{st}^o = -(\langle U_{ads} \rangle - RT)$, the corresponding adsorption energy is about 2 kJ mol^{-1} higher than that we obtain for chlorine radical. The isosteric heat of adsorption at 77 K for krypton in silicalite was measured by calorimetry[55] as 17.4 kJ mol^{-1}, corresponding to $\langle U_{ads} \rangle \sim -16.8$ kJ mol^{-1}, which compares well with the datum reported in Table 6 for bromine (−17.4 kJ mol^{-1}). The experimental value for the isosteric heat of adsorption of xenon in silicalite is[56] 26.6 ± 1 kJ mol^{-1} at 121 K, whence $\langle U_{ads} \rangle = -25.6$ kJ mol^{-1}, not far from the adsorption energy calculated for iodine (−27.8 kJ mol^{-1}).

Turning to the comparison with theoretical studies, it must be remarked that all the previous MD simulations of the Xe−silicalite system have been carried out with a fixed framework, which does not allow for the energy exchange between sorbates and zeolite; anyway, the agreement with our data is rather good. Pickett et al.[57] obtained $D = 1.86 \times 10^{-9}$ m^2 s^{-1} and $\langle U_{ads} \rangle = -26.9$ kJ mol^{-1}, again with 4 Xe atoms per unit cell; their D value is very close to that recently obtained by Jost *et al.*[58] for the same system. Xenon in silicalite at infinite dilution was simulated by June et al.[59] by turning off sorbate−sorbate interactions in a large system of 96 sorbates; they obtain

$D \sim 4 \times 10^{-9}$ m^2 s^{-1}, close to our value, along with a value of $\langle U_{ads} \rangle = -21$ kJ mol^{-1}, which is considerably different from all other sorption energy data, included ours. In ref 60 simulations of Ar and Xe at infinite dilution were carried out with a single diffusant, as in our case. The calculated adsorption energies for Xe (-27.8 kJ mol^{-1}) and Ar (-11.8 kJ mol^{-1}) are very close to our data for I and Cl, respectively. Their computed diffusion coefficients at 0 atoms/u.c. are seemingly too large, probably due to the too short trajectory length carried out for a *single* diffusant, which gives rise to very poor statistics.

To our knowledge, the only experimental or theoretical studies carried out so far on the diffusion of halogen molecules in the studied zeolites are the recent uptake measurements to complete loading of Kočiřík et al.:[61] they estimated the lower limit of the diffusion coefficient of iodine in silicalite as 10^{-12} m^2 s^{-1}, which is clearly not in contrast with our results. No experimental or simulation data are available on the diffusion of rare gases or halogen molecules in ZK4. However, the above comparison with the silicalite data shows that the present model is fairly reliable to study the diffusive process of the halogen species in neutral, all silica zeolites. Such equilibrium properties could also be helpful in the interpretation of the recombination data.

The diffusion coefficients obviously decrease going from chlorine to iodine, both for atomic and molecular species; the diatomic molecules move faster in silicalite, excluding bromine, whose diffusion coefficient is almost unchanged in the two silicates. This is rather surprising, because, on the basis of purely steric considerations, the passage of diatomic species through the ZK4 windows, which is the crucial step in the cage-to-cage diffusion, should slow the molecules compared to silicalite that does not present such "bottlenecks" for long-range diffusion. Moreover, one would expect that the difference in diffusion coefficients should further increase (in favor of silicalite) for larger diatomics. Actually, this is the case for chlorine and iodine: the last one shows a much larger decrease in D, going from silicalite to ZK4, than chlorine. It could be argued that the peculiar behavior of bromine, which seems not to be slowed at all in ZK4 compared to silicalite, may be somewhat connected to resonance effects between the breathing motion of the ZK4 windows and the molecular oscillations, which assist the molecule in the window-crossing step. Indeed, in ref 62 the spectral density of the ZK4 window diameters fluctuations were calculated by means of MD simulations: narrow peaks are present in the 350−400 cm^{-1} region, just above the equilibrium bromine frequency. For chlorine and iodine similar cooperative effects between the windows oscillations and the internal flexibility of the molecules do not significantly assist them in the crossing of the windows.

When we turn to the atomic, spherical species, the differences observed before between the diffusion coefficients in the two silicates mostly disappear. The diameters of the atomic species are considerably smaller than the kinetic diameter of corresponding diatomics, and then the passage through the windows is not as complicated and crucial as before. The diffusion of the atomic species in the two environments could have some influence on the recombination dynamics. If a species diffuses faster in a particular environment, the probability that the two atoms definitely separate shortly after the dissociation will increase. In this respect, looking at the percentages of OC events shown in Table 2, there are considerable differences between silicalite and ZK4, the first allowing an easier separation of atoms than the latter. However, in that case, we are dealing with the diffusion of highly excited atoms, while in the present one, where the diffusive properties of thermalized species are concerned, no differences are seemingly present. Therefore the peculiar features of the photodissociation−recombination process emphasize differences and properties which would not be apparent, or crucial, in an equilibrium simulation.

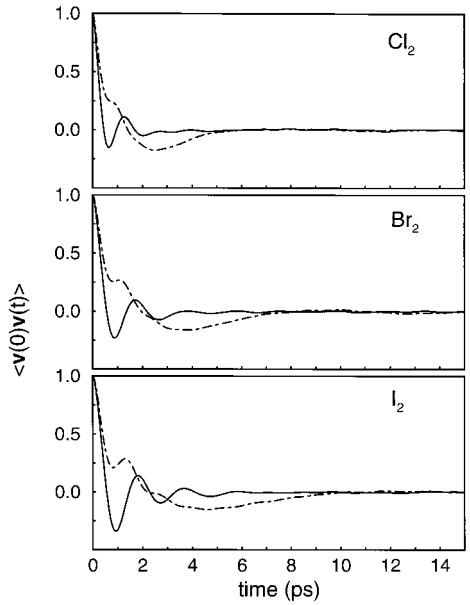

Figure 10. Center of mass velocity autocorrelation functions of the diatomic species; continuous lines: silicalite; dash−dotted lines: ZK4.

The center of mass−velocity autocorrelation functions (VACFs) for the diatomic molecules are reported in Figure 10. The VACFs in silicalite show a more liquid-like shape, with a sharp negative minimum at ∼1 ps, followed by an oscillatory trend and a more elastic behavior than those in ZK4. The walls of silicalite seem to act more effectively as backscatterers compared to ZK4, which gives rise only to a slight, positive oscillation at ∼1 ps, followed by a broad negative minimum. The examination of the VACF components in silicalite (not shown) points out that the deep minimum mainly results from the *z*-component, as the molecule−wall collisions usually occur perpendicularly to the axis of channels. Moreover, as Figure 10 shows, the backscattering is more effective for iodine, followed by bromine and chlorine—the heavier the molecule, the harder is the impact with the channel walls. This could be explained with a somewhat lower ability of the framework to absorb the impact when the colliding mass is much heavier compared to oxygen. This behavior may also be found in the sharper first oscillation of VACFs in ZK4, going from Cl_2 to I_2. The second, broad minimum characteristic of ZK4 VACF does extend to larger times for higher masses, ultimately leading to the lower observed diffusion coefficients.

The observed softer impact of the lighter molecules with the zeolite walls corresponds to a better ability of the framework to absorb and redistribute the collision energy. This is in agreement with the observed higher collision efficiency (ΔE *per collision* in Table 4) of the lighter diatomic species.

Figure 11 shows the Fourier transforms of the center of mass VACFs, which are useful tools to analyze the translational motions of the molecules. The two environments give rise to very different behaviors. The main peak in ZK4 extends to considerably lower frequencies than the main peak in silicalite. Moreover, the three diatomics show interesting differences. For chlorine in silicalite two peaks are present; the low-frequency band, roughly coinciding with the ZK4 one, is probably connected to the *shuttling* motion between intersections and channel centers.[63] The second peak arises from the rapid *rattling*

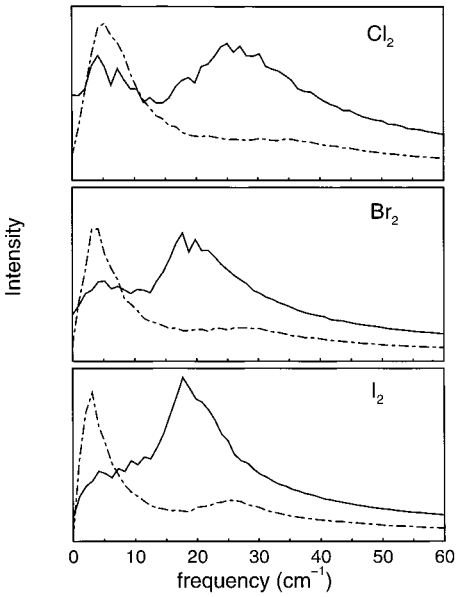

Figure 11. Fourier transform of the center of mass velocity autocorrelation functions of the diatomic species; continuous lines: silicalite; dash−dotted lines: ZK4.

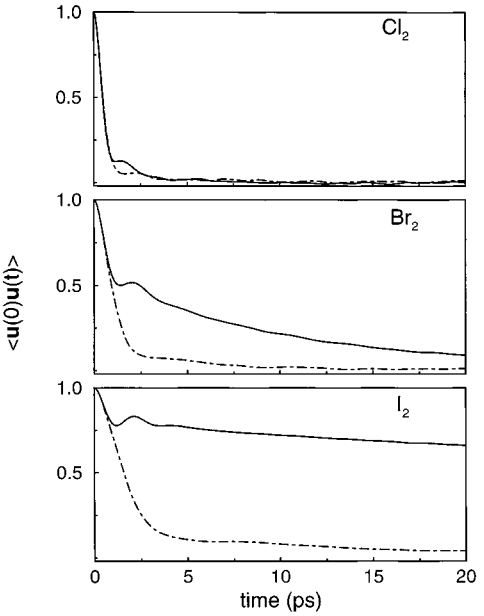

Figure 12. Orientational autocorrelation functions for the diatomic molecules; continuous lines: silicalite; dash−dotted lines: ZK4.

motion normal to the pore axis in silicalite: indeed, it mainly results from the *z*-component of the spectrum, not shown. Turning to bromine and then to iodine, the low-frequency peak in silicalite disappears, while in ZK4 a weak band around 25 cm^{-1}, absent for Cl_2, appears. In silicalite, for larger and heavier species, the longer-range (low-frequency) shuttling motions are considerably hindered and the main motion is that perpendicular to the walls. On the other hand, the intracage motions in ZK4 are not so heavily hindered for larger guests and the low-frequency peak is always present.

Further information on the dynamics of sorbate−zeolite systems can be gained following the decorrelation of the unit vector $\hat{\mathbf{u}}(t)$, parallel to the bond, and thus suitable to describe the orientation of the diatomic molecules in the pore network. The autocorrelation of this vector, $P_1(t)$ (first Legendre polynomial), defined as

$$P_1(t) = \langle \hat{\boldsymbol{u}}(t) \cdot \hat{\boldsymbol{u}}(0) \rangle \tag{4}$$

decays exponentially to zero with a slope depending on the rate of change in orientation, i.e., on the loss of orientational memory. Figure 12 shows the calculated functions for the three halogen molecules; in ZK4 the molecules have more space available to rotate, thus the decorrelation of $P_1(t)$ is always faster, compared to silicalite. While, on one hand, the two $P_1(t)$ curves are rather similar in the chlorine case, the relative differences are much more marked going to bromine and iodine, which experience considerable hindered rotations in silicalite. The channel structure forces the larger molecules to remain roughly aligned with the channel axes, thus keeping their orientation unchanged for longer times. This increased hindering of rotations with increasing molecular dimensions is much less marked in ZK4, for which the orientational memory remains short-ranged also in the iodine case, where after 10 ps $P_1(t)$ already decays to zero.

The greater rotational freedom experienced by chlorine in silicalite may have influence on the low probability of a definitive separation of the chlorine atoms after the dissociation, which has been remarked in the previous section (Table 2). Indeed, if a molecule is roughly aligned to the channel axis at the dissociation time, the two atoms will be pushed in opposite directions, along the direction of the channel and their separation will be more likely. But, in the case of chlorine, the molecule may often be placed more or less transversely in the channels, so that after the dissociation the atoms will immediately collide with walls, and their recombination will be more probable, as observed in silicalite.

The peculiar structure of silicalite entails that the decorrelation of the *x*-component of $P_1(t)$ is mostly associated with molecules initially in the sinusoidal channels that move in the straight ones; similarly, the migration from straight to sinusoidal channels determines the decay of the *y*-component. Obviously, the *z*-component decay is faster, as there are no channels in such direction: therefore the *z*-component of $\hat{\boldsymbol{u}}(t)$ is generally small (because the molecule is mostly aligned along *x* or *y*) and quickly oscillates around zero, leading to a fast decorrelation. June and co-workers[63] found that for butane the decorrelation is faster along *y* than along *x*, both decays being considerably slow. In the present study, we find a behavior similar to that of butane only for iodine (Figure 13), while for Cl_2 and Br_2 the decay rates along *x* and *y* are rather fast and similar to each other. The interconversion between straight and zigzag channels plays a key role in the understanding of the diffusion of flexible, nonspherical sorbates in silicalite, and the probabilities of events like the straight-to-zigzag migration, or vice versa, can be directly connected to the diffusion coefficients by means of a statistical approach.[64] Further calculations are presently under way to illuminate this topic.

5. Conclusions

The results presented in this paper provide new, general data on the effects of different confining geometries on the dynamics of reactive and diffusive processes of diatomic molecules. We have investigated the guest−host dynamical coupling at the level of the recombination reactions of photodissociated radical species and diffusion of diatomic molecules in two topologically different zeolites: silicalite and ZK4. In particular, we have examined two factors ruling the mechanism of the reactive and diffusive phenomena: lattice dynamics, acting as an effective heat bath for the sorbed molecules, and the effects of two different crystal structures. However, the underlying assumption

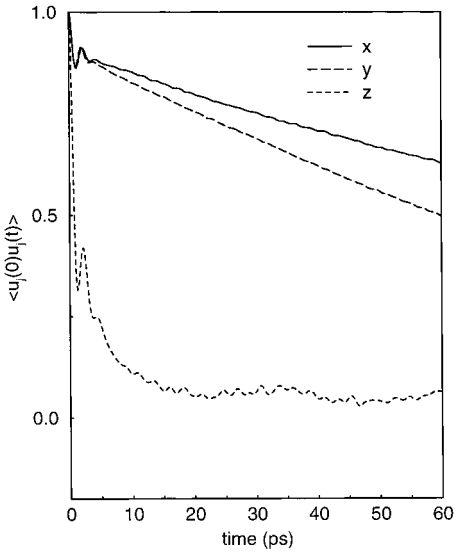

Figure 13. Components of the orientational autocorrelation function for iodine in silicalite.

of the present paper is that a purely classical treatment of vibrational energy relaxation might provide a reasonable representation of relevant features of the adsorbate−zeolite system.[65] Our results seem to bear out this simplification, at least at a qualitative level. Obviously more work is needed to understand the very details of the vibrational energy relaxation in zeolites and a quantum mechanical treatment should be essential.

Greater recombination percentages in ZK4, in particular for the larger atoms, result from a more effective confinement compared to the more "open" silicalite structure. Interestingly, the percentage of reactive trajectories shown by iodine in ZK4 (64%) is closer to the result previously obtained for a liquid solvent[37] (80%), than to the silicalite datum (35%). The cage structure of ZK4, characterized by narrow windows with diameter comparable to the dimensions of the guest species, determines its ability to hold the photodissociated radicals inside the same α-cage, in particular for the larger iodine atoms. The energy dissipation of the excited radicals, immediately following the dissociation, seems to be the most important step in determining the overall recombination process. In this respect, both collision and energy exchange data show a better efficiency of silicalite, thus explaining many of the observed phenomena, such as the higher probability of simple reactions in silicalite, or the faster recombination of chlorine. On the other hand, the vibrational relaxation of the formed molecules seems not to be as crucial as one might suspect. However, a straightforward interpretation of the relaxation of the excited molecules, both in the short- and long-time regimes, is complicated to achieve. Simple resonance rules between vibrational modes are not easily applicable because of the considerable deviations of the excited oscillator frequency from its equilibrium value. Moreover, additional, system-specific effects such as the collision frequency have proven to heavily affect the system behavior. The examination of vibrational spectra of the excited molecules allowed to partially illuminate this problem.

Some interesting features regarding the mobility and the guest−host interactions of the molecular and atomic species involved in the studied reactions have been illuminated through equilibrium MD simulations. On one hand some features present in the reactive dynamics are most probably connected to the shift from equilibrium imposed by the dissociation, and thus they have not been observed in the equilibrium simulations; on the other hand some equilibrium properties such as the VACFs and the first Legendre polynomials allowed a better understanding of the overall dissociation−recombination process.

Acknowledgment. We are grateful to MURST, University of Sassari and Consiglio Nazionale delle Ricerche for financial support.

References and Notes

(1) *Proceedings of the 12th International Zeolite Conference*, Baltimore, 1998; Treacy, M. M. J., Marcus, B. K., Bisher, M. E., Higgins, J. B., Eds.; Material Research Society: Warrendale, 1999.
(2) *Modeling of Structure and Reactivity in Zeolites*; Catlow, C. R. A., Ed.; Academic Press: London, 1992.
(3) Demontis, P.; Suffritti, G. B. *Chem. Rev.* **1997**, *97*, 2845.
(4) *Molecular Dynamics in Restricted Geometries*; Klafter, J., Drake, J. M., Eds.; John Wiley & Sons: New York, 1989.
(5) Owrutsky, J. C.; Raftery, D.; Hochstrasser, R. M. *Annu. Rev. Phys. Chem.* **1994**, *45*, 519.
(6) Onda, K.; Yaginuma, M.; Yokota, T.; Wada, A.; Domen, K.; Hirose, C.; Kano, S. S. *J. Chem. Phys.* **1998**, *108*, 5935.
(7) Liu, Q.; Wang, J.-K.; Zewail, A. H. *Nature* **1993**, *364*, 427.
(8) Wang, J.-K.; Liu, Q.; Zewail, A. H. *J. Phys. Chem.* **1995**, *99*, 11309.
(9) Hoffman, G. J.; Sekreta, E.; Apkarian, V. A. *Chem. Phys. Lett.* **1992**, *191*, 401.
(10) Chang, L.-C.; Song, T.-T.; Tai, C.-C.; Su, T.-M. *J. Phys. Chem.* **1996**, *100*, 13548.
(11) Song, T. T.; Su, T.-M. *J. Phys. Chem.* **1996**, *100*, 13554.
(12) Harris, A. L.; Berg, M.; Harris, C. B. *J. Chem. Phys.* **1986**, *84*, 788.
(13) Smith, D. E.; Harris, C. G. *J. Chem. Phys.* **1987**, *87*, 2709.
(14) Zadoyan, R.; Sterling, M.; Apkarian, V. A. *J. Chem. Soc., Faraday Trans.* **1996**, *92*, 1821.
(15) Ali, D. P.; Miller, W. H. *J. Chem. Phys.* **1983**, *78*, 6640.
(16) Batista, V. S.; Coker, D. F. *J. Chem. Phys.* **1996**, *105*, 4033.
(17) Baldoví, M. V.; Corma, A.; García, H.; Martí, V. *Tetrahedron Lett.* **1994**, *35*, 9447.
(18) Corma, A.; Fornés, V.; García, H. *J. Am. Chem. Soc.* **1994**, *116*, 2276.
(19) Li, X.; Ramamurthy, V. *Tetrahedron Lett.* **1996**, *37*, 5235.
(20) Pitchumani, K.; Warrier, M.; Cui, C.; Weiss, R. G.; Ramamurthy, V. *Tetrahedron Lett.* **1996**, *37*, 6251.
(21) Lem, G.; Kaprinidis, A.; Schuster, D. I.; Ghatlia, N. D.; Turro, N. J. *J. Am. Chem. Soc.* **1993**, *115*, 7009.
(22) Leibovitch, M.; Olovsson, G.; Sundarababu, G.; Ramamurthy, V.; Scheffer, J. R.; Trotter, J. *J. Am. Chem. Soc.* **1996**, *118*, 1219.
(23) Alvaro, M.; Corma, A.; García, H.; Miranda, M. W.; Primo, J. *J. Chem. Soc.: Chem. Commun.* **1993**, *13*, 1041.
(24) Blatter, F.; Frei, H. *J. Am. Chem. Soc.* **1994**, *116*, 1812.
(25) Cizmeciyan, D.; Sonnichsen, L. B.; Garcia-Garibay, M. A. *J. Am. Chem. Soc.* **1997**, *119*, 184.
(26) Sun, H.; Blatter, F.; Frei, H. *J. Am. Chem. Soc.* **1996**, *118*, 6873.
(27) Pitchumani, K.; Warrier, M.; Ramamurthy, V. *J. Am. Chem. Soc.* **1996**, *118*, 9428.
(28) García, H.; García, S.; Scaiano, J. C. *J. Phys. Chem.* **1996**, *100*, 18158.
(29) Corma, A.; García, H.; Iborra, S.; Martí, V.; Miranda, M. A.; Primo, J. *J. Am. Chem. Soc.* **1993**, *115*, 2177.
(30) Chang, C. D. *Hydrocarbons from methanol*; Marcel Dekker: New York, 1983.
(31) Blaszkowski, S. R.; van Santen, R. A. *J. Am. Chem. Soc.* **1997**, *119*, 5020, and references therein.
(32) Alba, M. D.; Romero, A. A.; Occelli, M. L.; Klinowski, J. *J. Phys. Chem. B* **1997**, *101*, 5166.
(33) Harris, A. L.; Brown, J. K.; Harris, C. B. *Annu. Rev. Phys. Chem.* **1988**, *39*, 341.
(34) Zadoyan, R.; Sterling, M.; Ovchinnikov, M.; Apkarian, V. A. *J. Chem. Phys.* **1997**, *107*, 8446.
(35) Chachisvilis, M.; Garcia-Ochoa, I.; Douhal, A.; Zewail, A. H. *Chem. Phys. Lett.* **1998**, *293*, 153.
(36) Douhal, A.; Fiebig, T.; Chachisvilis, M.; Zewail, A. H. *J. Phys. Chem. A* **1998**, *102*, 1657.
(37) Delogu, F.; Demontis, P.; Suffritti, G. B.; Tilocca, A. *J. Chem. Phys.* **1998**, *109*, 2865.
(38) van Koningsveld, H.; van Bekkum, H.; Jansen, J. C. *Acta Cryst. B* **1987**, *43*, 127.
(39) Pluth, J. J.; Smith, V. J. *J. Am. Chem. Soc.* **1980**, *102*, 4704.
(40) El Amrani, S.; Vigné-Maeder, F.; Bigot, B. *J. Phys. Chem.* **1992**, *96*, 9417.

(41) Kiselev, A. V.; Du, P. Q. *J. Chem. Soc., Faraday Trans. 2* **1981**, *77*, 1.
(42) Herzberg, G. *Spectra of Diatomic Molecules*; Van Nostrand Reinhold: New York, 1950.
(43) Song, T.-T.; Hwang, Y. S.; Su, T. M. *J. Phys. Chem. A* **1997**, *101*, 3860.
(44) Amar, F. G.; Berne, B. J. *J. Phys. Chem.* **1984**, *88*, 6720.
(45) Demontis, P.; Suffritti, G. B.; Quartieri, S.; Fois, E. S.; Gamba, A. *J. Phys. Chem.* **1988**, *92*, 867.
(46) Demontis, P.; Suffritti, G. B.; Tilocca, A. *J. Chem. Phys.* **1996**, *105*, 5586.
(47) Demontis, P.; Suffritti, G. B. *Chem. Phys. Lett.* **1994**, *223*, 355.
(48) Swope, W. C.; Andersen, H. C.; Berens, P. H.; Wilson, K. R. *J. Chem. Phys.* **1982**, *76*, 637.
(49) Nesbitt, D. J.; Hynes, J. T. *J. Chem. Phys.* **1982**, *77*, 2130.
(50) Schwartz, B. J.; King, J. C.; Zhang, J. Z.; Harris, C. B. *Chem. Phys. Lett.* **1993**, *203*, 503.
(51) Chitra, R.; Yashonath, S. *J. Phys. Chem. B* **1997**, *101*, 5437.
(52) Heink, W.; Karger, J.; Pfeifer, H.; Stallmach, F. *J. Am. Chem. Soc*. **1990**, *112*, 2175.
(53) Rees, L V. C.; Shen, D. *J. Chem. Soc., Faraday Trans.* **1990**, *86*, 3687.
(54) Dunne, J. A.; Mariwala, R.; Rao, M.; Sircar, S.; Gorte, R. J.; Muers, A. L. *Langmuir* **1996**, *12*, 5888.
(55) Llewellyn, P. L.; Coulomb, J.-P.; Grillet, Y.; Patarin, J.; Lauter, H.; Reichert, H.; Rouquerol, J. *Langmuir* **1993**, *19*, 1846.
(56) Bülow, M.; Härtel, U.; Müller, U.; Unger, K. K. *Ber. Bunsen-Ges. Phys. Chem.* **1990**, *94*, 74.
(57) Pickett, S. D.; Nowak, A. K.; Thomas, J. M.; Peterson, B. K.; Swift, J. F. P.; Cheetham, A. K.; den Ouden, C. J. J.; Smit, B.; Post, M. F. M. *J. Phys. Chem.* **1990**, *94*, 1233.
(58) Jost, S.; Bär, N.-K.; Fritzsche, S.; Haberlandt, R.; Kärger, J. *J. Phys. Chem. B* **1998**, *102*, 6375.
(59) June, R. L.; Bell, A. T.; Theodorou, D. N. *J. Phys. Chem.* **1990**, *94*, 8232.
(60) El Amrani, S.; Vigné-Maeder, Bigot, B. *J. Phys. Chem.* **1992**, *96*, 9417.
(61) Kočiřík, M.; Kornatowski, J.; Masařík, V.; Novák, P.; Zikánová, A.; Maixner, J. *Microporous Mesoporous Mater.* **1998**, *23*, 295.
(62) Demontis, P.; Suffritti, G. B. In *Zeolites and Related Microporous Materials, Studies in Surface Science and Catalysis*, Vol. 84; Weitkamp, J., Karge, H. G., Pfeifer, H., Hölderich, W., Eds.; Elsevier: Amsterdam, The Netherlands, 1994; pp 2107−2113.
(63) June, R. L.; Bell, A. T.; Theodorou, D. N. *J. Phys. Chem.* **1992**, *96*, 1051.
(64) Kärger, J.; Demontis, P.; Suffritti, G. B.; Tilocca, A. *J. Chem. Phys.* **1999**, *110*, 1163.
(65) Egorov, S. A.; Berne, B. J. *J. Chem. Phys.* **1997**, *107*, 6050.